NEUTRINO TRANSPORT IN STRONGLY MAGNETIZED PROTO-NEUTRON STARS AND THE ORIGIN OF FAST SPINNING PULSAR KICKS

By

TESFAYE TEKLEHAIMANOT

A THESIS SUBMITTED TO
THE DEPARTMENT OF PHYSICS

PRESENTED IN PARTIAL FULFILLMENT OF THE REQUIREMENTS
FOR THE DEGREE OF MASTER OF SCIENCE IN PHYSICS

ADDIS ABABA UNIVERSITY
ADDIS ABABA,ETHIOPIA

JUNE 2013

ADDIS ABABA UNIVERSITY
SCHOOL OF GRADUATE STUDIES

This is to certify that the thesis prepared by **TESFAYE TEKLEHAIMANOT**, entitled "**NEUTRINO TRANSPORT IN STRONGLY MAGNETIZED PROTO-NEUTRON STARS AND THE ORIGIN OF FAST SPINNING PULSAR KICKS**" and submitted in partial fulfillment of the requirements for the degree of **Master of Science in physics** compiles with the regulations of the University and meets the accepted standards with respect to originality.

Signed by the Examining Committee:

Examiner: Prof A.V.Gholap Signature:______ Date:__________
Examiner: Prof P.Singh Signature:______ Date:__________
Advisor: Dr.Legesse W. Signature:______ Date:__________

Abstract

The Fermi LAT collaboration has recently reported the discovery of the pulsations of the γ-ray pulsar J1823-3021A with a luminosity which is the highest observed to date for any millisecond pulsar (MSP). This large luminosity implies a large spin down rate $\dot{P}$ and therefore a large magnetic field which seems to be incompatible with the observed short rotation period P . In proto-neutron stars with strong magnetic fields, the cross section for ν_e ($\bar{\nu}_e$) absorption on neutrons (protons) depends on the local magnetic field strength resulting from the quantization of energy levels for the e^- (e^+) produced in the final state. If the neutron star possesses an asymmetric magnetic field topology in the sense that the magnitude of magnetic field in the north pole is different from that in the south pole, then asymmetric neutrino emission may be generated. We calculate the absorption cross sections of ν_e and $\bar{\nu}_e$ in strong magnetic fields as a function of the neutrino energy. These cross sections exhibit oscillatory behaviors that occur because new Landau levels for the e^- (e^+) become accessible as the neutrino energy increases. By evaluating the appropriately averaged neutrino opacities, we demonstrate that the change in the local neutrino flux caused by the modified opacities is rather small. To generate appreciable kick velocity ($\sim$300 km s^{-1}) to the newly formed neutron star, the difference between the field strengths at the two opposite poles of the star must be at least 10^{16} G. We also consider the magnetic field effect on the spectral neutrino energy fluxes. The oscillatory features in the absorption opacities give rise to modulations in the emergent spectra of ν_e and $\bar{\nu}_e$.

Acknowledgements

First of all, I would like to thank the almighty God for letting me to accomplish this study.

Secondly, I would like to thank Dr.Legesse Wotro K., my advisor, for his many suggestions and constant support during this research.

Finally, I wish to thank the following: Mekdes Chernet (my wife);Samuel Tesfaye, Nardos Tesfaye and my family.

Addis Ababa University Tesfaye
June 2013

Table of Contents

Abstract **iii**

Acknowledgements **iv**

Table of Contents **v**

1 Introduction **1**

1.1 Previous Works on Asymmetric Neutrino Emission Induced by Magnetic Fields . . . 3

1.2 Plan of This Thesis . . . 6

2 Fast-Spinning Star **7**

2.1 Exotic,fast-spinning star . . . 8

2.2 Looking in gamma-ray light . . . 9

3 Effect of Asymmetric Magnetic Field Topology **11**

3.1 ν_e And $\bar{\nu}_e$ Absorption Cross Sections In Strong Magnetic Fields . . 11

3.1.1 The Cross Sections . . . 12

3.1.2 Thermal Averaging . . . 16

3.1.3 Limiting Cases . . . 17

3.1.4 Discussion . . . 18

3.2 Neutrino Transport Near The Stellar Surface . . . 20

3.3 Rosseland Mean Opacities . . . 23

3.4 Differential Neutron Fluxes And neutron Star Kick From Asymmetric Magnetic Field Topology . . . 26

3.4.1 Asymmetric Emission of Neutrinos from a Proto-Neutron star 28

3.5 Magnetic Field Effect On ν_e And $\bar{\nu}_e$ Energy Spectra . . . 32

4 Conclusion **35**

References **37**

List of Figures

2.1 This still from a NASA animation depicts the super bright and super young pulsar J1823-3021A, which is the brightest and youngest pulsar yet discovered, and has a powerful magnetic field. The pulsar spins about The object pulses 183.8 times a second and is located about 27,000 light years from Earth. 8

2.2 This plot shows the positions of nine new pulsars (magenta) discovered by Fermi and of an unusual millisecond pulsar (green) the youngest such object known found by the Fermi Gamma Ray Space Telescope. With this new batch of discoveries, Fermi has detected more than 100 pulsars in gamma rays. 9

2.3 This image shows the on and off state of gamma rays from pulsar J1823-3021A as seen by Fermi's Large Area Telescope (LAT) .The object pulses 183.8 times a second and has a spin period of 5.44 milliseconds, which translates to 11,000 rpm. 10

3.1 Absorption cross section (per nucleon) of ν_e,$(1 - Y_e)$ $\sigma_B^{(abs)}(E_\nu)$, in units of $A \times MeV^2 = \pi G^2 cos^2\theta_c(c_V^2 + 3c_A^2)MeV^2 \simeq 0.91 \times 10^{-42}cm^2$, as a function of the neutrino energy. The dashed line is the zero-field result (The effect of the nucleon thermal motion is included but is hard to discern). The heavy and the light solid lines are the results for b = 100, with and without the effect of the nucleon thermal motion, respectively. The dotted line is the elastic scattering cross section, $\sigma_B^{(sc)}(E_\nu)$, in the same units. All results are for T = 3 MeV, Y_e=0.1, and μ_e=20 MeV (corresponding to $7.2 \times 10^{11} gcm^{-3}$). 14

3.2 Absorption cross section (per nucleon) of $\bar{\nu}_e$, $Y_e\sigma_B^{(abs)}(E_\nu)$. The physical parameters, units, and labels are the same as in Fig.3.1. . . 15

3.3 Absorption cross sections (per nucleon) of ν_e (left) and $\bar{\nu}_e$ (right), in units of A $\times$ $MeV^2 = \pi G_F^2 cos^2\theta_c(c_V^2 + 3c_A^2) \times MeV^2 \simeq 0.91 \times 10^{-42} cm^2$, as functions of the neutrino energy for different physical parameters. All results assume $Y_e = 0.1$. The solid, short-dashed, long-dashed, and dot-dashed curves are for (b, μ_e /MeV, T /MeV) = (100, 20, 3), (100, 10, 3), (200, 20, 3), and (100,20,5), respectively. [Note that for $\bar{\nu}_e$, the curve for (b, μ_e /MeV, T /MeV) = (100, 10, 3) is almost identical to the curve for (b, μ_e /MeV, T /MeV) = (100, 20, 3), and both curves are close to the curve for (b, μ_e /MeV, T /MeV) = (100, 20, 5).] The light dotted lines are the elastic scattering cross sections in the same units. 18

3.4 Ratio of the Rosseland mean opacity $\kappa_R^{(B)}$ of ν_e to its zero- field value $\kappa_R^{(0)}$ as a function of the magnetic field strength $b = B/B_c$ (with $B_c = 4.414 \times 10^{13}$ G). All results assume $Y_e = 0.1$. The heavier curves correspond to T $=T_\nu = 3$ MeV, and the lighter cures correspond to T $= T_\nu = 5$ MeV. Thel solid, short-dashed, and long-dashed lines are for $\mu_e = 10$, 15, and 20 MeV, respectively. 24

3.5 Ratio of the Rosseland mean opacity $\kappa_R^{(B)}$ of ν_e to its zero- field value $\kappa_R^{(0)}$ as a function of the magnetic field strength $b = B/B_c$ (with $B_c = 4.414 \times 10^{13}$ G). All results assume $Y_e = 0.1$ and μ_e=20 MeV (but the results are rather insensitive to the value of μ_e). The solid, short-dashed, and long-dashed lines are for T=$T_\nu = 3$, 5, and 7 MeV, respectively. 25

3.6 Illustrative examples of the ν_e spectral energy fluxes (in arbitrary units) modified by the magnetic fields. The light solid, short-dashed,and long-dashed lines are for b = 0, 100, and 300, respectively. The light dotted line is the Fermi-Dirac spectrum with T = $T_{eff} = 3$ MeV. 33

Chapter 1

Introduction

The pulsar J1823-3021A, located in the globular cluster NGC 6624, was discovered in 1994 (Biggs et al.1990. 1994). It has been recognized shortly after the discovery of pulsars that neutron stars have velocities much in excess of those of any other normal stellar populations in our Galaxy (Gunn and Ostriker 1970 ; Minkowski 1970). However, it is only in the last few years that a significant body of evidence has come into place to support the view that Type II supernovae are nonspherical and that neutron stars receive large kick velocities at birth. Lyne and Lorimer (1994) analyzed pulsar velocities in light of new proper-motion measurements (Harrison, Lyne, and Anderson 1993) and up-to-date pulsar distance scale (Taylor and Cordes 1993), and they concluded that pulsars were born with a mean speed of ∼450 km s^{-1}, much larger than previously thought. More recent studies of pulsar velocities have adopted more sophisticated statistical methods and included better treatment of selection effects and uncertainties (Lorimer, Bailes, and Harrison 1997 ; Hansen and Phinney 1997 ; Cordes and Cherno 1997).

They all yielded a result for the pulsar birth velocity in qualitative agreement (although not in quantitative details) with that of Lyne and Lorimer (1994). In particular, Cordes and Chernof (1997) found that the three dimensional space velocities of their sample of 47 pulsars have a bimodal distribution, with characteristic speeds of 180 km s^{-1} and 700 km s^{-1} (corresponding to 80 % and 20 % of the population). They also estimated that pulsars with velocities greater than 1000 km s^{-1} may be under represented owing to selection effects in pulsar surveys (The uncertainty in the high velocity end of the pulsar velocity distribution function has also been emphasized by Hansen and Phinney 1997). Concrete evidence for the existence of pulsars with velocities of $\gtrsim$1000 km s^{-1} has come from the observation of the Guitar Nebula pulsar (B2224+65), which produces a bow shock when plowing through the interstellar medium (Cordes,Romani, and Lundgren 1993). In addition, studies of pulsar supernova remnant associations have uncovered a number of pulsars having velocities much greater than 1000 km s^{-1} (Frail, Goss, and Whiteoak 1994), although in many cases the associations are not completely secur.

Compelling evidence for supernova asymmetry and pulsar kicks also comes from the detection of geodetic precession in the binary pulsar PSR 1913+16 (Cordes, Wasserman, and Blaskiewicz 1990) and the orbital plane precession in the PSR J0045-7319/B star binary (Lai, Bildsten, and Kaspi 1995 ; Kaspi et al. 1996) and its fast orbital decay (which indicates retrograde rotation of the B star with respect to the orbit ; see Lai 1996). These results demonstrate that binary break up (as originally suggested by Gott, Gunn, and Ostriker 1970 ; see Iben and Tutukov 1996) cannot be solely responsible for the observed pulsar velocities and that natal kicks are required. In addition, evolutionary studies of neutron star binary population imply the existence of pulsar kicks (Deway and Cordes 1987 ;Fryer and Kalogera 1997 ; Fryer, Burrows, and Benz 1998 ; see also Brandt and Podsiadlowski 1995). Finally, there are alarge number of direct observations of nearby supernovae (see, e.g., Cropper et al. 1988 ; Trammell, Hines, and Wheeler 1993 ; McCray 1993 ; Utrobin, Chugai, and Andronova 1995) and supernova remnants (Morse, Winkler, and Kirshner 1995 ; Aschenbach, Egger, and Trumper 1995) in radio, optical, and X-ray bands, which supports the notion that supernova explosions are not spherically symmetric.

The origin of the pulsar velocities is still unknown. Two classes of mechanisms for the natal kicks have been suggested. The first class relies on convective instabilities in the collapsed stellar core and within the rebounding shock (Burrows and Fryxell 1992 ; Burrows, Hayes, and Fryxell 1995 ; Janka and Muller 1994, 1996 ; Herant et al. 1994). The asymmetries in the matter and temperature distributions associated with the instabilities naturally lead to asymmetric matter ejection and/or asymmetric neutrino emission. Numerical simulations indicate that the local, post collapse instabilities are not adequate to account for kick velocities higher than a few hundred km s^{-1} (Janka and Muller 1994). A variant of this class of models therefore relies on the global asymmetric perturbations seeded in the presupernova cores (Goldreich et al. 1996 ; see also Bazan and Arnett 1994). Clearly, the magnitude of kick velocity depends on the degree of initial asymmetry in the imploding core (Burrows and Hayes 1996). Because of various uncer tainties in the presupernova stellar models, it is not clear at this point whether sufficiently large initial perturbations can be produced in the precollapse core (Lai and Goldreich 1998).

In this thesis we focus on the second class of models in which the large pulsar kick velocities arise from asymmetric neutrino emission induced by strong magnetic fields. Since 99% of the neutron star binding energy (a few times 10^{53} ergs) is released in neutrinos, tapping the neutrino energy would appear to be an efficient means to kick the newly formed neutron star. Magnetic fields are naturally invoked to break the spherical symmetry in neutrino emission. But the actual mechanism is unclear. We first briefly comment on previous works on this and related subjects.

1.1 Previous Works on Asymmetric Neutrino Emission Induced by Magnetic Fields

A number of authors have noted that parity violation in weak interactions may lead to asymmetric neutrino emission from proto-neutron stars (Chugai 1984 ; Dorofeev et al. 1985 ; Vilenkin 1995 ; Horowitz and Piekarewicz 1997). However, their studies are largely unsatisfactory for a number of reasons : they either failed to identify the most relevant neutrino emission/interaction processes or the relevant physical conditions in proto-neutron stars, or stopped at estimating the magnetic field effects on neutrino opacities. Chugai (1984) and Vilenkin (1995) (see also Bezchastnov and Haensel 1996) considered neutrino-electron scattering and concluded that the effect is extremely small (e.g., to obtain V_{kick}= 300 km s^{-1} would require a magnetic field of at least kick 10^{16} G). However, neutrino-electron scattering is less important than neutrino-nucleon scattering in determining the characteristics of neutrino transport in proto-neutron stars. Similarly, Dorofeev et al. (1985) considered neutrino emission by Urca processes in strong magnetic fields. But as shown by Lai and Qian (1998), in the bulk interior of the neutron star, the asymmetry associated with neutrino emission is cancelled by the asymmetry associated with neutrino absorption.

Concerning the parity violation effect in proto-neutron stars, Horowitz and Li (1997) recently suggested that the asymmetry in neutrino emission may be enhanced owing to multiple scatterings of neutrinos by nucleons that are slightly polarized by the magnetic field. They estimated that a field strength of few times 10^{12}G is adequate to account for kick velocities of a few hundred km s^{-1}. However, the paper by Horowitz and Li (1997) only discusses the idealized situations of scattering media and ignores various essential physics that is needed in a proper treatment of neutrino transport in proto-neutron stars. In particular, it does not consider the effect of neutrino absorption, which one might suspect to wash out the cumulative effect from multiple scatterings. Our own study of the parity violation effect (Lai and Qian 1998) was flawed in the treatment of scattering terms in the neutrino transport equation. As shown by Arras and Lai (1998),detailed balance requires that there be no cumulative effect from multiple scatterings in the bulk interior of the proto-neutron star where local thermodynamic equilibrium applies to a good approximation. Enhancement of neutrino emission asymmetry from multiple scatterings obtains only after neutrinos thermally decouple from proto-neutron star matter and therefore is insignificant.

Bisnovatyi-Kogan (1993) attributed pulsar kicks to asymmetric magnetic field distribution in proto-neutron stars. Using the fact that neutron decay rate can be modified the magnetic field, the inferred that neutrino emissions from opposite sides of the neutron star surface are different. However, neutron decay is not directly relevant for neutrino emission from a newly formed neutron star. Roulet (1997) (whose paper was posted while this paper was being written) considered the relevant neutrino absorption processes. But his study was restricted to calculating the neutrino cross sections as functions of neutrino energy (corresponding to § 3.1 of this paper) and therefore was insufficient for addressing the issue of asymmetric neutrino emission.

Finally, it is worthwhile to mention a speculative idea on pulsar kicks that relies on nonstandard neutrino physics. Kusenko and Segre (1996) suggested that asymmetric ν_τ emission could result from the Mikheyev-Smirnov-Wolfenstein flavor transformation between ν_τ and ν_e inside a magnetized proto-neutron star because a magnetic field changes the resonance condition for the flavor transformation. With a ν_τ mass of $\sim$100 eV, they claimed that magnetic fields of 3×10^{14} G can give the pulsar a kick velocity of a few hundred km s^{-1}. However, their treatment of neutrino transport was over simplified : e.g., they ignored that neutrinos of different energies have different resonance surfaces. Furthermore, a simple geometric effect and realistic proto-neutron star conditions easily reduce their estimated kick velocity by an order of magnitude. Most likely, a magnetic field strength of $\sim 10^{16}$ G is needed to produce the observed average pulsar kick velocity via their mechanism (see Qian 1997). Similarly strong magnetic fields are required in variants of the Kusenko and Segre mechanism, e.g., those considered by Akhmedov, Lanza, and Sciama (1997) (which relies on both the neutrino mass and the neutrino magnetic moment to facilitate the flavor transformation).

1.2 Plan of This Thesis

As should be clear from the brief review in § 1.1, in spite of quite a number of suggestions, there is at present no consensus on the magnitudes of the magnetic field induced asymmetry in neutrino emission from proto-neutron stars and the resulting kick velocities. In this paper we study the effect of asymmetric magnetic field topology on pulsar kicks. Since the energy levels of e^- and e^+ in a magnetic field are quantized, the ν_e and $\bar{\nu_e}$ absorption opacities near the neutrinosphere and the neutrino-matter decoupling region depend on the local magnetic field strength. If the magnitude of magnetic field in the north pole is different from that in the south pole (the field does not need to be ordered), then asymmetric neutrino flux may be generated. Here we ignore the effects of magnetic fields on the proto-neutron star structure through the equation of state-these are secondary effects as far as neutrino transport is concerned.

The organization of this thesis is as follows. In section 2 we observed that Fast-Spinning Star J1823-3021A. In section 3.1 we calculate the ν_e and $\bar{\nu_e}$ absorption cross sections as functions of neutrino energy in strong magnetic fields. Section 3.2 summarizes the basic features of neutrino transport near the neutron star surface. In section 3.3 we derive and evaluate the "Rosseland mean " neutrino opacities, which are directly related to the local neutrino flux. We then consider in section 3.4 the change in neutrino flux caused by the modified opacities, estimate the kick velocity and magnetic field resulting from an asymmetric magnetic field topology.In section 3.5 we briefly consider how the emergent neutrino spectra may be modified by the strong magnetic field. Finally, we present our conclusion.

Unless noted otherwise, we shall use units in which $\hbar$, c, and the Boltzmann constant k are unity.

Chapter 2

Fast-Spinning Star

The spinning star, a millisecond pulsar called J1823-3021A, is located inside a packed conglomeration of stars called a globular cluster about 27,000 light years from Earth in the constellation Sagitarrius. The pulsar emits incredibly intense high energy gamma rays, which the researchers detected and studied using NASA's Fermi Gamma Ray Space Telescope. Their analysis suggests the pulsar is just 25 million years old a baby as far as these stars go, for millisecond pulsars tend to be a billion years old or so, researchers said. The pulsar's extreme brightness and youth challenge current ideas about how super bright millisecond pulsars form and how widespread they may be,researchers said. "These anomalously energetic millisecond pulsars must be forming at a rate similar to the previously known, more normal millisecond pulsars at least in globular clusters, but possibly in the whole universe as well," said study lead author Paulo Freire of the Max Planck Institute for Radio Astronomy in Bonn,Germany. "In a sense, this pulsar would be the proverbial tip of a hidden new iceberg.

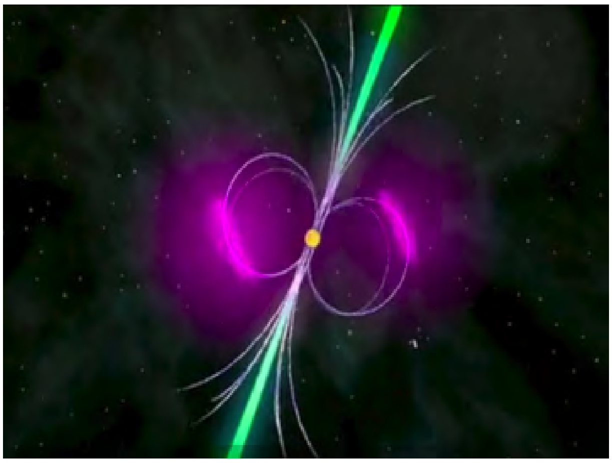

Figure 2.1: This still from a NASA animation depicts the super bright and super young pulsar J1823-3021A, which is the brightest and youngest pulsar yet discovered, and has a powerful magnetic field. The pulsar spins about The object pulses 183.8 times a second and is located about 27,000 light years from Earth.

2.1 Exotic,fast-spinning star

Pulsars form when massive stars die in supernova explosions and their remnants collapse into compact objects made only of the particles called neutrons. When a mass as great as our sun's is packed into a space the size of a city, the conserved angular momentum causes the resulting neutron star to spin very rapidly and to emit a ray of high energy light that sweeps around like a lighthouse beam. This light appears to pulse because astronomers see the beam only when it's pointed at Earth. "Normal"pulsars rotate at a rate between 7 and 3,750 revolutions per minute, but millisecond pulsar can spin much faster up to 43,000 rotations per minute. These hyper-spinners are thought to be revved up by accretion of matter from a companion star. Indeed, roughly 80 percent of millisecond pulsars discovered to date are found in binary systems, researchers said. The new study could shed some more light on these exotic objects. The research is detailed online in the Nov. 3 issue of the journal Science.In a separate study, astronomers announced the discovery of nine previously unknown gamma-ray pulsars, also using the Fermi space telescope.

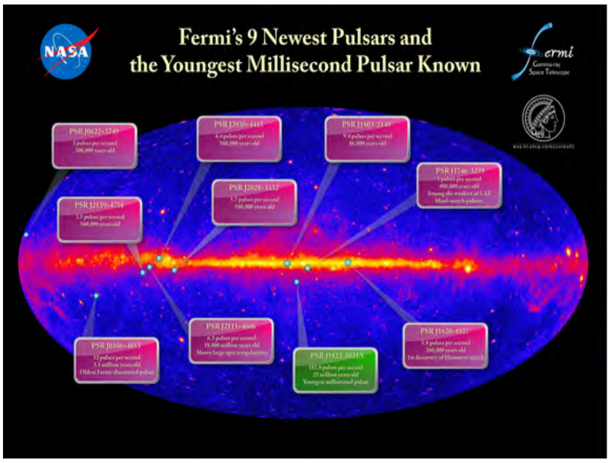

Figure 2.2: This plot shows the positions of nine new pulsars (magenta) discovered by Fermi and of an unusual millisecond pulsar (green) the youngest such object known found by the Fermi Gamma Ray Space Telescope. With this new batch of discoveries, Fermi has detected more than 100 pulsars in gamma rays.

2.2 Looking in gamma-ray light

For the J1823-3021A study, researchers trained the Fermi space telescope on the globular cluster NGC 6624. Globular clusters are good places to look for millisecond pulsars, because the dense packing of stars facilitates the formation of binary systems. Freire and his colleagues picked up a lot of gamma ray emission from the cluster so much that they initially thought the light was coming from 100 or so millisecond pulsars. But that wasn't the case."We now find that all detectable gamma ray emission comes from one single millisecond pulsar," Freire told Space.com in an email.That pulsar is J1823-3021A, which is spinning at about 11,100 revolutions per minute, or one complete turn every 5.44 milliseconds. The team didn't discover the pulsar; it has been known since the 1990s. But its incredible gamma ray brightness remained undetected until now.

J1823-3021A also appears to have a much stronger magnetic field than other millisecond pulsars. The exotic object's combination of characteristics is likely to have astronomers scratching their heads, Freire said. "It challenges the way we believe millisecond pulsars form," he said. "It was not thought that, for the spin period of this object (5.44 ms), they could be so energetic and have such a high magnetic field."

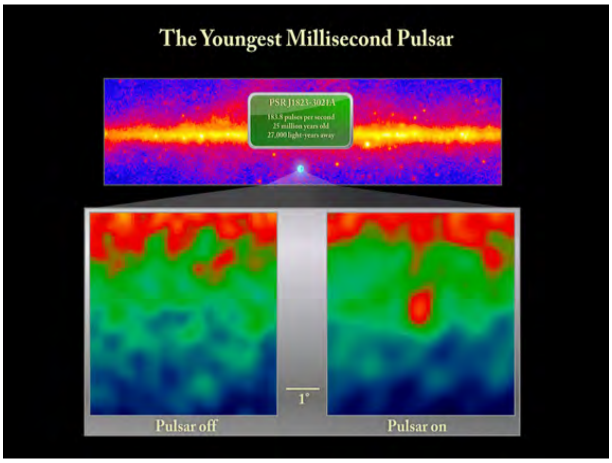

Figure 2.3: This image shows the on and off state of gamma rays from pulsar J1823-3021A as seen by Fermi's Large Area Telescope (LAT) .The object pulses 183.8 times a second and has a spin period of 5.44 milliseconds, which translates to 11,000 rpm.

Its amazing that all of the gamma rays we see from this cluster are coming from a single object. It must have formed recently based on how rapidly its emitting energy. Its a bit like finding a screaming baby in a quiet retirement home, said Paulo Freire, the studys lead author, at the Max Planck Institute for Radio Astronomy in Bonn, Germany.

Chapter 3

Effect of Asymmetric Magnetic Field Topology

A different kick mechanism relies on the asymmetric magnetic field distribution in proto-neutron stars (see Bisnovatyi-Kogan 1993; however, he considered neutron decay, which is not directly relevant for neutrino emission from proto-neutron stars). Since the cross section for ν_e ($\bar{\nu}_e$) absorption on neutrons (pro tons) depends on the local magnetic field strength due to the quantization of energy levels for the e^- (e^+) produced in the final state, the local neutrino fluxes emerged from different regions of the stellar surface are different. Calculations indicate that to generate a kick velocity of $\sim 300kms^{-1}$ using this mechanism alone would require that the difference in the field strengths at the two opposite poles of the star be at least 10^{16} G (Lai and Qian 1998b). Note that unlike the kick due to parity violation, this mechanism does not require the magnetic field to be ordered, i.e., only the magnitude of the field matters.

3.1 ν_e And $\bar{\nu}_e$ Absorption Cross Sections In Strong Magnetic Fields

In this section we consider how magnetic fields modify the (total) neutrino absorption (ν_e+n$\rightarrow$ p+e^- and $\bar{\nu}_e$+p$\rightarrow$n+e^+) cross sections for specific neutrino energies. We present our calculation of the ν_e absorption cross section in detail. The $\bar{\nu}_e$ absorption cross section can be obtained in a similar manner.

To begin with, it is useful to review various energy scales involved in the problem. Near the neutrinosphere and the neutrino-matter decoupling region, the matter density is typically 10^{11}-10^{12} g cm^{-3}, and the temperature is about several MeV. The electrons are extremely relativistic and highly degenerate, with Fermi energy $E_{F,e} \simeq 51.5\ (Y_e\rho_{12})^{1/3}$ MeV, where Y_e ~0.1 is the electron fraction (the number electron per nucleon) and ρ_{12}=$\rho/(10^{12} gcm^{-3})$. The neutrons and protons have Fermi energies $E_{F,n}$= $1.4[(1$-$Y_e)\rho_{12}]^{2/3}$ MeV, and $E_{F,p}$=$1.4(Y_e\rho_{12})^{2/3}$ respectively, and thus they are essentially nondegenerate.

3.1.1 The Cross Sections

In strong magnetic fields the transverse motion of the electron is quantized into Landau levels. The electron energy dispersion relation is

$$E_e = [p_z^2 + m_e^2(1 + 2nb)]^{1/2}, \qquad n = 0, 1, 2, ..., \tag{3.1.1}$$

where p_z is the longitudinal momentum (along the magnetic field), and n is the Landau level index. The dimensionless field strength b is defined as

$$b \equiv \frac{B}{B_c}, \qquad with\ B_c = \frac{m_e^2 c^3}{\hbar e} = 4.414 \times 10^{13} G. \tag{3.1.2}$$

[B_c is the critical field strength defined by equating the cyclotron energy $\hbar eB/(m_e c)$ to $m_e c^2$.] The quantization effect on the proton is extremely small because of the large proton mass and is neglected throughout this paper.

Since the cyclotron radius (characterizing the size of the Landau wavefunction) $[\hbar c/(eB)]^{1/2} = [\hbar/(m_e c)]b^{1/2} = 386 b^{-1/2}$ fm is much greater than the range of the weak interaction [$\hbar/(m_w c) \simeq 2.5 \times 10^{-3}$ fm, where $m_w \simeq 80$ GeV is the mass of W boson], one can use the V -A theory with contact interaction. Locally (at the point of interaction) the Landau wavefunction resembles a plane wave. Thus, we expect that the spin-averaged matrix element is the same as in the case without magnetic fields. This expectation has been borne out by detailed calculations (see, e.g., Fassio Canuto 1969 ; Matese and O'Connell 1969). Therefore, we only need to consider the effect of magnetic field on the electron phase space.

Since the neutrino energy (a few to tens of MeV) of interest is much less than the nucleon mass, we first consider the case where the nucleon mass is taken to be infinity, an approximation adopted in the standard zero-field calculations (Tubbs and Schramm 1975). The cross section for ν_e+n$\rightarrow$p+e^- can be written as a sum over the (spatial and spin) states of the electron (per unit volume)

$$\sigma_B^{(abs)}(E_\nu) = A\sum_e (1-f_e)\delta(E_\nu + Q - E_e), \tag{3.1.3}$$

where we have defined

$$A \equiv \pi G_F^2 cos^2\theta_c(c_v^2 + 3c_A^2), \tag{3.1.4}$$

and the other symbol have their usual meanings: $G_F = (293GeV)^{-2}$ is the universal Fermi constant, $cos^2\theta_c = 0.95$ refers to the Cobbibo angle, $c_v = 1$ and $c_A = 1.26$ are coupling constants, $Q = m_n - m_p = 1.293$ MeV is the neutron-proton mass difference, E_ν is the ν_e energy, and $(1-f_e)$ is the pauli blocking factor. The electron occupation number f_e is

$$f_e = \frac{1}{exp[(E_e - \mu_e)/T] + 1} \tag{3.1.5}$$

where E_e is the electron energy, μ_e is the electron chemical potential, and T is the matter temperature. For zero-field, the sum becomes $2\int d^3p/(2\pi)^3$, and we have

$$\sigma_{B=0}^{(abs)}(E_\nu) = \frac{A}{\pi^2}(E_\nu + Q)[(E_\nu + Q)^2 - m_e^2]^{1/2}(1-f_e), \tag{3.1.6}$$

with $E_e = E_\nu + Q$. For $B \neq 0$, knowing that the degeneracy of the landau level (per unit area) is $g_n eB/hc = g_n m_e^2 b/(2\pi)$, with $g_n = 1$ for n=0 and $g_n = 2$ for n>0,we have

$$\begin{aligned}\sigma_B^{(abs)}(E_\nu) &= A\int_{-\infty}^{\infty}\frac{dp_z}{2\pi}\sum_n g_n\frac{m_e^2 b}{2\pi}(1-f_e)\delta(E_\nu + Q - E_e)\\ &= A\frac{m_e^2 b}{2\pi^2}\sum_{n=0}^{n_{max}} g_n\frac{E_e}{p_{z,n}}(1-f_e),\end{aligned} \tag{3.1.7}$$

where $E_e = E_\nu + Q$, and $p_{z,n} = [E_e^2 - m_e^2(1+2nb)]^{1/2}$. The upper limit n_{max} for the sum is the maximum value of n for which $p_{z,n}$ is meaningfully defined,i.e,

$$n_{max} = Int\left[\frac{(E_\nu + Q)^2 - m_e^2}{2m_e^2 b}\right] \tag{3.1.8}$$

where Int[x] stands for the integral part of x . Henceforth, n_{max} is similarly defined, and we shall not explicitly write out the lower and upper limits for the sum.

Figure 3.1, depicts $\sigma_B^{(abs)}(E_\nu)$ for b=100 and $\sigma_B^{(abs)}(E_\nu)$ as functions of E_ν for

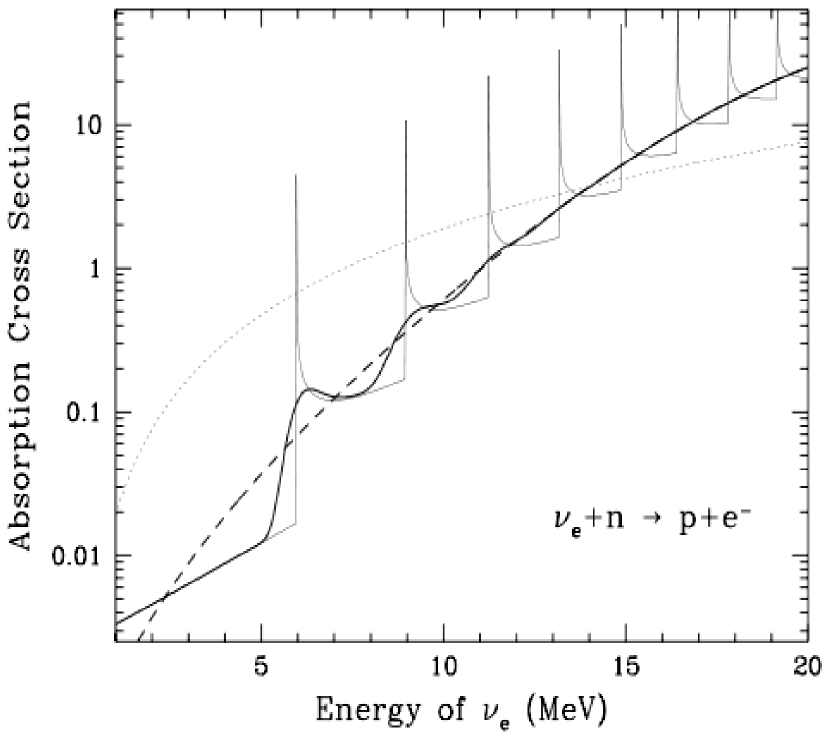

Figure 3.1: Absorption cross section (per nucleon) of ν_e,$(1 - Y_e)$ $\sigma_B^{(abs)}(E_\nu)$, in units of $A \times MeV^2 = \pi G^2 cos^2\theta_c(c_V^2 + 3c_A^2)MeV^2 \simeq 0.91 \times 10^{-42}cm^2$, as a function of the neutrino energy. The dashed line is the zero-field result (The effect of the nucleon thermal motion is included but is hard to discern). The heavy and the light solid lines are the results for b = 100, with and without the effect of the nucleon thermal motion, respectively. The dotted line is the elastic scattering cross section, $\sigma_B^{(sc)}(E_\nu)$, in the same units. All results are for T = 3 MeV, Y_e=0.1, and μ_e=20 MeV (corresponding to $7.2 \times 10^{11} gcm^{-3}$).

typical conditions ($Y_e = 0.1, \mu_e =$ 20MeV, and T=3MeV) in aproto-neutron star. Note that ideally,one should compare $\sigma_B^{(abs)}(E_\nu)$ and $\sigma_{B=0}^{(abs)}(E_\nu)$ at the same matter density. For $\mu_e \simeq E_{F,e} \gg T$(so that $n_e^- \gg n_e^+$), the matter density is related to μ_e via

$$\rho = \frac{m_n}{Y_e}\frac{1}{\pi^2}\int_0^\infty p^2 dp f_e \qquad (for B = 0). \tag{3.1.9}$$

$$\rho = \frac{m_n}{Y_e}\frac{m_e^2 b}{2\pi^2}\int_0^\infty dp_z \sum_n g_n f_e \qquad (for B \neq 0). \tag{3.1.10}$$

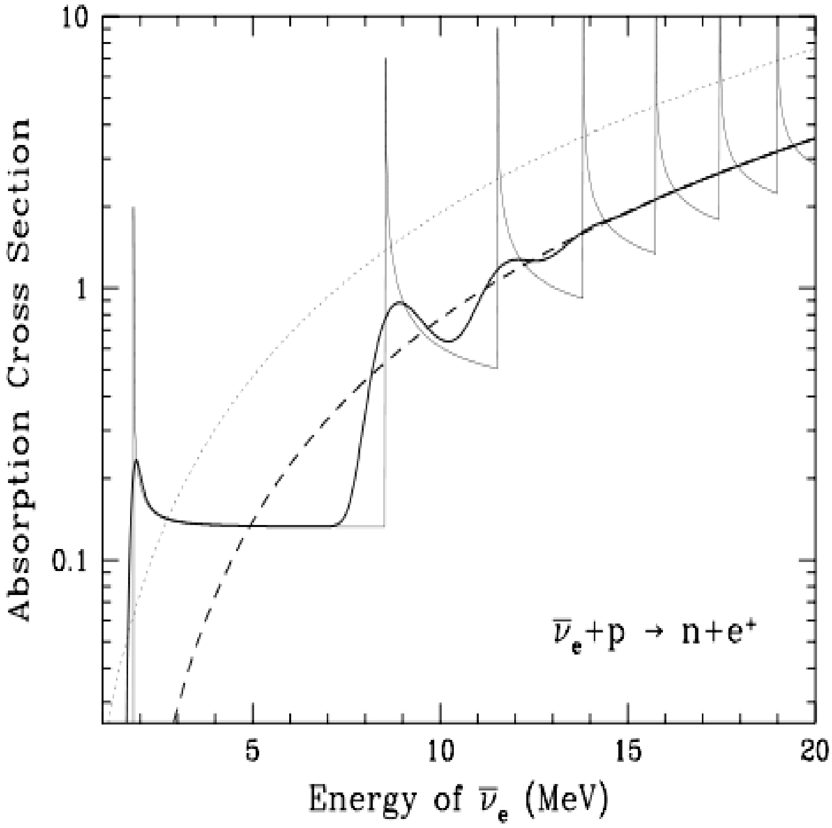

Figure 3.2: Absorption cross section (per nucleon) of $\bar{\nu}_e$, $Y_e\sigma_B^{(abs)}(E_\nu)$. The physical parameters, units, and labels are the same as in Fig.3.1.

In practice, we have found that for a given μ_e , the dependence of ρ on the field strength is rather weak for the range of parameters of interest in this paper. Thus, in all of our calculations here and below, we compare the cross sections at a given μ_e . A prominent feature of $\sigma_B^{(abs)}(E_\nu)$ shown in Figure 3.1. is the presence of " resonances," which occur when $p_{z,n}$= 0 (eq. [3.1.7]), i.e., at the neutrino energies for which the final state electron lies in a " stationary " Landau level (with zero longitudinal momentum). These resonances reflect the divergence of the density of states of electrons at these stationary Landau levels.

The cross section for $\bar{\nu}_e$ +p→n+e^+ can be similarly calculated. One only needs to replace Q with -Q and μ_e with $-\mu_e$ in the expressions for ν_e absorption to obtain the desired expressions for $\bar{\nu}_e$ absorption. The numerical results for $\bar{\nu}_e$ absorption cross section are shown for Figure 3.2. for the same physical parameters as used for Figure 3.1.

3.1.2 Thermal Averaging

The divergent cross sections at the "resonances" shown in Figures 3.1. and 3.2. are clearly unphysical. They are smoothed out by the thermal motion of the neutron. To the leading order, the width of the resonance is $(kT/m_n)^{1/2}\ E_\nu$, corresponding to the Doppler shift of the neutrino energy in the neutron's rest frame. The recoil energy, of order E_ν^2/m_n, is much less effective in smoothing out the resonances and will be neglected. With this approximation, the smoothed cross section can be written as

$$\langle\sigma_B^{(abs)}(E_\nu)\rangle \simeq \frac{1}{(2\pi)^2}\int \upsilon_n^2\ d\upsilon_n\ f_n \int d\ cos\ \theta_n\ \sigma_B^{(abs)}(E_\nu^{'}), \tag{3.1.11}$$

where $E_\nu^{'} = E_\nu(1-\upsilon_n cos\theta_n)$ and $f_n = (2nm/T)^{3/2}\ exp(-m\upsilon_n^2/2T)$ is the velocity distribution function for the neutron. If we replace the factor $(1-f_e)$ [which depends on $(E_\nu^{'}+Q)$] in $\sigma_B^{(abs)}(E_\nu^{'})$ with the average value $\langle 1-f_e\rangle$, which can be approximately taken as $(1-f_e)$ evaluated at $E_e = E_\nu +$ Q, then the angular integral in equation (3.1.11)can be carried out analytically. For B = 0, we have

$$\langle\sigma_{B=0}^{(abs)}(E_\nu)\rangle \simeq \frac{A}{(2\pi)^2}\ \langle 1-f_e\rangle\ \int \upsilon_n\ d\upsilon_n\ f_n \frac{1}{3\pi^2 E_\nu}$$

$$\times(E_e^2-m_e^2)^{3/2}\Big|_{E_e-E_{\nu(1-\upsilon_n)+Q}}^{E_e} = E_\nu^{(1+\upsilon_n)+Q}, \tag{3.1.12}$$

which is reduced to

$$\langle\sigma_{B=0}^{(abs)}(E_\nu)\rangle \simeq \frac{A}{\pi^2}(E_\nu+Q)^2\langle 1-f_e\rangle \times \left[1+\left(\frac{E_\nu}{E_{\nu+Q}}\right)^2\frac{T}{m_n}\right], \tag{3.1.13}$$

if we neglect the electron mass m_e. For $B \neq 0$, we find

$$\langle\sigma_B^{(abs)}(E_\nu)\rangle \simeq \frac{A}{(2\pi)^2}\langle 1-f_e\rangle \int \upsilon_n d\upsilon_n f_n \frac{m_e^2 b}{2\pi^2 E_\nu}$$

$$\times\sum_n g_n[E_e^2-m_e^2(1+2nb)]^{1/2}\Big|_{E_e=E_\nu(1-\upsilon_n)+Q}^{E_e} = E_\nu^{(1+\upsilon_n)+Q} \tag{3.1.14}$$

We could have approximately included the neutron recoil effect by replacing Q and Q-$(E_\nu+Q)^2/(2m_n)$ in equations(3.1.12)-(3.1.14). But we choose to leave out this effect since as mentioned previously, it is ineffective in smoothing out the resonances in $\sigma_B^{(abs)}(E_\nu)$. We have numerically evaluated equations (3.1.12) and (3.1.14), and the results are depicted in Figure 3.1., together with the cross section are shown in Figure 3.2. As expected, we find that for B=0,the averaged cross section $\langle\sigma_{B=0}^{(abs)}(E_\nu)\rangle$ is almost identical to $\sigma_{B=0}^{(abs)}(E_\nu)$ (see eq. [3.1.13]). However, for $B \neq 0$,the thermal averaging is essential in obtaining the smoothed physical absorption cross sections.

3.1.3 Limiting Cases

The oscillatory behaviors of $\langle\sigma_B^{(abs)}(E_\nu)\rangle$ for Figures 3.1. and 3.2. can be demonstrated analytically. Using the Poisson summation formula (Ziman 1979) :

$$\sum_{n=0}^{\infty} f(n+\frac{1}{2}) = \sum_{s=-\infty}^{\infty} (-1)^s \int_0^\infty f(f) e^{2\pi i s x} dx, \tag{3.1.15}$$

we can rewrite the sum in equation (3.1.14) as

$$m_e^2 b \sum_n g_n [E_e^2 - m_e^2(1+2nb)]^{1/2} = \frac{2}{3}(E_e^2 - m_e^2)^{3/2}$$

$$+(2m_e^2 b)^{3/2} Re \sum_{s=1}^{\infty} \frac{1-i}{4\pi i s^{3/2}} exp\left[2\pi i s(\frac{E_e^2 - m_e^2}{2m_e^2 b})\right]. \tag{3.1.16}$$

The first term on the right-hand side of equation (3.1.16) corresponds to the zero-field result, and the second term (involving the sum of many oscillatory terms) corresponds to the correction owing to the quantization effect. The sum is clearly convergent, and thus for small B the averaged cross section $\langle\sigma_B^{(abs)}(E_\nu)\rangle$ is reduced to the zero-field value $\langle\sigma_{B=0}^{(abs)}(E_\nu)\rangle$

For sufficiently large B at a given E_ν , or, equivalently, for sufficiently small E_ν at a given B, only the ground state Landau level is filled by the electron, i.e., $n_{max} = 0$ (see eq [3.1.8]). In this limit, $\langle\sigma_B^{(abs)}(E_\nu)\rangle > \langle\sigma_{B=0}^{(abs)}(E_\nu)\rangle/4$, and only the first term in equation (3.1.7) needs to be retained. We then have

$$\langle\sigma_B^{(abs)}(E_\nu)\rangle \simeq A\frac{m_e^2 b}{2\pi^2}\frac{(E_\nu + Q)}{[(E_\nu+Q)^2 - m_e^2]^{1/2}}(1-f_e) \tag{3.1.17}$$

for ν_e absorption. A similar expression for $\bar{\nu}_e$ absorption is obtained by replacing Q with -Q and μ_e with $-\mu_e$ in equation(3.1.17).

3.1.4 Discussion

The physical conditions that Figures 3.1 and 3.2 are based on (T = 3 MeV, $Y_e =$ 0.1, and $\mu_e = 20$ MeV, corresponding to a matter density of $\rho = 7.2 \times 10^{11} gcm^{-3}$) are typical of the neutrinosphere of the proto-neutron star. In Figure 3.3, we plot the ν_e and $\bar{\nu}_e$ absorption cross sections for a number of slightly different physical parameters, specified by b, μ_e and T (all with $Y_e = 0.1$). The cross section for elastic neutral current scattering $\nu + N \to \nu + N$, $\sigma^{sc}(E_\nu) \simeq G_F^2 E_\nu^2/\pi$ (Tubbs and Schramm 1975), is also shown for comparison. Absorption dominates the transport of ν_e for high energies, with the ratio of absorption to scattering cross sections per nucleon (1 -Y_e)$\sigma^{(abs)}/\sigma^{(sc)}$ approaching for $E_\nu \gg \mu_e$. For smaller

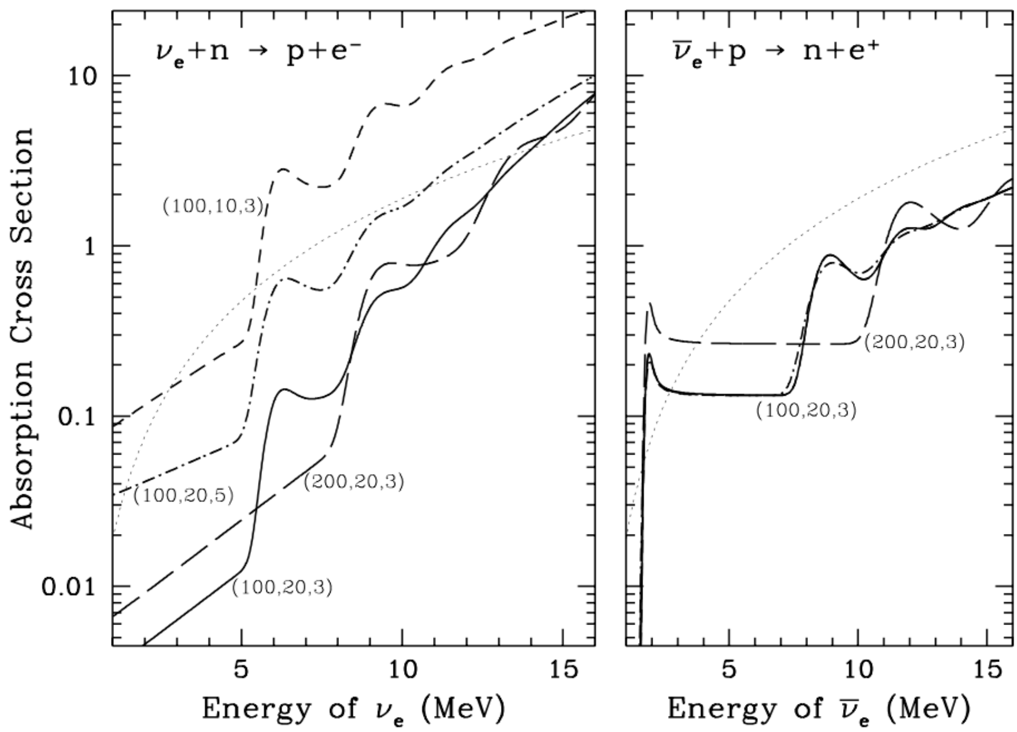

Figure 3.3: Absorption cross sections (per nucleon) of ν_e (left) and $\bar{\nu}_e$ (right), in units of A $\times$ $MeV^2 = \pi G_F^2 cos^2\theta_c(c_V^2 + 3c_A^2) \times MeV^2 \simeq 0.91 \times 10^{-42} cm^2$, as functions of the neutrino energy for different physical parameters. All results assume $Y_e = 0.1$. The solid, short-dashed, long-dashed, and dot-dashed curves are for (b, μ_e /MeV, T /MeV) = (100, 20, 3), (100, 10, 3), (200, 20, 3), and (100,20,5), respectively. [Note that for $\bar{\nu}_e$, the curve for (b, μ_e /MeV, T /MeV) = (100, 10, 3) is almost identical to the curve for (b, μ_e /MeV, T /MeV) = (100, 20, 3), and both curves are close to the curve for (b, μ_e /MeV, T /MeV) = (100, 20, 5).] The light dotted lines are the elastic scattering cross sections in the same units.

energies ($E_\nu \lesssim \mu_e$), absorption is severely suppressed by the Pauli blocking of the final electron states, and scattering becomes more important. In the case of $\bar{\nu}_e$, Pauli blocking is negligible, and scattering almost always dominates the transport, with the ratio of scattering to absorption cross section per nucleon $\sigma^{(sc)}/[Y_e\sigma^{(abs)}] \simeq 2(0.1/Y_e)$ for $E_\nu \gtrsim 10$ MeV.

As we can see from Figures 3.1-3.3, for a given set of physical parameters of the medium ($T,\ Y_e,\ \mu_e\ or\ \rho$), the magnetic field effect on the absorption opacity is more prominent for lower energy neutrinos than for higher energy ones. This is because for a given field strength, as the neutrino energy increases, more and more Landau levels become available for the electron in the final state (see eq. [3.1.8]). Consequently, the electron phase space and hence the cross section should approach the zero-field values according to the correspondence principle. We found that typically when the number of Landau levels filled by the electron (n_{max}) is greater than 2-3, the magnetic field effect on the absorption opacity becomes negligible. The "critical " neutrino energy is approximately given by

$$E_\nu^{crit} \simeq m_e(2bn_{max}+1)^{1/2} \simeq 6\left(\frac{n_{max}}{3}\right)^{1/2}\left(\frac{B}{10^{15}G}\right)^{1/2} MeV. \qquad (3.1.18)$$

for $E_\nu \gtrsim E_\nu^{(crit)}$, one can approximate $\langle\sigma_B^{(abs)}(E_\nu)\rangle$ by the zero-field value $\langle\sigma_{B=0}^{(abs)}(E_\nu)\rangle$ with good accuracy (within a few percent). Alternatively, we can define a threshold magnetic field, B_{th}, above which the ν_e and $\bar{\nu}_e$ absorption opacities are modified (by more than a few percent) by the magnetic field:

$$B_{th} \simeq \frac{\langle E_\nu\rangle^2}{2n_{max}m_e^2}B_c \simeq 3\times10^{15}\left(\frac{\langle E_\nu\rangle}{10MeV}\right)^2 \left(\frac{3}{n_{max}}\right)G, \qquad (3.1.19)$$

where $\langle E_\nu\rangle$ ~10 MeV is the average neutrino energy.

In the deeper layers of the neutron star, the typical neutrino energy is higher. Therefore, we expect the magnetic field effect on the absorption opacities to be smaller there. In addition, for ν_e , absorption becomes unimportant as compared to scattering in the high-density region (although not necessarily in the deepest interior, where ν_e can be degenerate). Thus, in order to assess the importance of the magnetic field effect on the neutrino emission, we only need to focus on the surface region, the region between the neutrinosphere and the neutrino-matter decoupling layer. We note that because the absorption opacities in the magnetic field for different neutrino energies oscillate around the zero-field values, without a detailed calculation of the mean opacity (appropriately averaged over the neutrino energy spectrum) one cannot even answer the qualitative question such as whether the magnetic field increases or decreases the local neutrino energy flux.

In section 3.1-3.3, we study how the modified absorption cross sections affect the emergent ν_e and $\bar{\nu}_e$ energy fluxes and spectra from the proto-neutron star.

3.2 Neutrino Transport Near The Stellar Surface

As discussed in section 3.1.4, the quantization effect of magnetic fields on neutrino absorption is important in the region only near the neutron star surface (between the neutrino sphere and the neutrino-matter decoupling layer). In this section we consider neutrino transport in this relatively low-density region.

Because ν_e and $\bar{\nu}_e$ with typical energies of 10 MeV have comparable absorption and scattering opacities (see Fig. 3.3), the emergent ν_e and $\bar{\nu}_e$ energy fluxes and spectra are determined essentially in the same region where these two neutrino species just begin to thermally decouple from the proto-neutron star matter. The ν_e and $\bar{\nu}_e$ occupation numbers in this region are then approximately given by

$$f_{\nu_e}(E_\nu) = \frac{1}{exp[(E_\nu/T) - \eta_\nu] + 1}, \tag{3.2.1}$$

and

$$f_{\bar{\nu}_e}(E_\nu) = \frac{1}{exp[(E_\nu/T) + \eta_\nu] + 1}, \tag{3.2.2}$$

respectively, where $\eta_\nu = \mu_\nu/T$, and μ_ν is the ν_e chemical potential. From these occupation numbers, we obtain

$$n_{\nu_e} - n_{\bar{\nu}_e} = \frac{\eta_\nu}{6}\left(1 + \frac{\eta_\nu^2}{\pi^2}\right)T^3, \tag{3.2.3}$$

and

$$U_{\nu_e} + U_{\bar{\nu}_e} = \frac{7\pi^2}{120}\left(1 + \frac{30\eta_\nu^2}{7\pi^2}\right)T^4, \tag{3.2.4}$$

where for example, n_{ν_e} and U_{ν_e} are the number and energy densities,respectively,for the ν_e. We can estimate the magnitude of η_ν as follows. The net deleptonization rate of the proto-neutron star is

$$-\dot{N}_e \sim \frac{Y_{e,i}M/m_N}{t_{diff}} \sim c(n_{\nu e} - n_{\bar{\nu} e})\pi R^2, \tag{3.2.5}$$

where $Y_{e,i}$ is the initial electron fraction of the proto-neutron star, M is the proto-neutron star mass, m_N is the nucleon mass, t_{diff} is the neutrino diffusion time-scale, and R is the proto-neutron star radius. The sum of the ν_e and $\bar{\nu}_e$ luminosities is

$$L_{\nu_e} + L_{\bar{\nu}_e} \sim \frac{1}{3}\frac{GM^2/R}{t_{diff}} \sim c(U_{\nu_e} + U_{\bar{\nu}_e})\pi R^2 \tag{3.2.6}$$

From equations(3.2.3)-(3.2.6), we have

$$\begin{aligned} \eta_\nu &\sim \frac{21\pi^2}{20}\frac{1 + (30/7\pi^2)\eta_\nu^2 + (15/7\pi^4)\eta_\nu^4}{1 + (\eta_\nu^2/\pi^2)} \\ \frac{Y_{e,i}TR}{GMm_N} &\sim 0.1\left(\frac{Y_{e,i}}{0.36}\right)\left(\frac{T}{5MeV}\right) \ll 1, \end{aligned} \tag{3.2.7}$$

where the numerical value is obtained for $M \simeq 1.4M_\odot$ and $R \simeq 10$ km. Therefore, to a good approximation, the ν_e and $\bar{\nu}_e$ in the decoupling region have Fermi-Dirac energy distributions with zero chemical potentials.

Let $I_E = I_E(r, \hat{\Omega})$ be the specific intensity of neutrinos of a given species, where r is the spatial position, and $\hat{\Omega}$ specifies the direction of propagation. The general transport equation takes the form

$$\begin{aligned} \hat{\Omega}\cdot \nabla I_E = \rho\kappa_E^{(abs)*} I_E^{(FD)} + \rho\kappa_E^{(sc)}\frac{1}{4\pi}\int d\Omega' I_E' \\ -\rho[\kappa_E^{(abs)*} + \kappa_E^{(sc)}]I_E, \end{aligned} \tag{3.2.8}$$

where $I_E^{'} = I_E(r, \hat{\Omega}^{'})$, and the subscript "E "indicates that the relevant physical quantities depend on the neutrino energy E. The opacities $\kappa_E^{(abs)*}$ and $\kappa_E^{(sc)}$ are related to the corresponding cross sections as, e.g., $\kappa_E^{(abs)*} = (1 - Y_e)\sigma_E^{(abs)*}/m_N$ and $\kappa_E^{(sc)} = \sigma^{(sc)}/m_N$ for ν_e . Note that we have included the effect of stimulated absorption for neutrinos (Imshennik and Nadezhin 1973) by introducing the corrected absorption opacity $\kappa_E^{(abs)*} = \kappa_E^{(abs)}(1 + exp(-E/T))$ (T is the matter temperature). Here after, we shall suppress the superscript $''*''$ in $\kappa_E^{(abs)*}$, and the notation $\kappa_E^{(abs)}$ should be understood as having included the correction due to stimulated absorption. The quantity $I_E^{(FD)}$ in equation (3.2.8) is the equilibrium neutrino intensity, given by the Fermi-Dirac distribution

$$I_E^{(FD)} = \frac{E^3}{c^2 h^3} \frac{1}{exp(E/T) + 1}. \tag{3.2.9}$$

Note that the time derivative term $(\partial I_E/\partial t)$ on the left-hand side of equation (3.2.8) has been neglected. This corresponds to an instantaneous redistribution of emission and absorption sources (i.e., an instantaneous redistribution of matter temperature). The timescale for the redistribution is of order the mean free path divided by c, much smaller than the neutrino cooling time of the star.

The zeroth-order moment of the transport equation can be written as

$$\nabla \cdot F_E = \rho \kappa_E^{(abs)} c (U_E^{(FD)} - U_E), \tag{3.2.10}$$

where $F_E \int I_E \hat{\Omega} d\Omega$ is the (spectral) neutrino energy flux, $U_E = \int I_E d\Omega/c$ is the energy density, and $U_E^{(FD)} = (4\pi/c) I_E^{(FD)}$ is the corresponding equilibrium energy density. With Eddington closure relation, the first moment of equation (3.2.8) becomes

$$F_E = -\frac{c}{3\rho\kappa_E^{(t)}} \nabla U_E, \tag{3.2.11}$$

where $\kappa_E^{(t)} = \kappa_E^{(abs)} + \kappa_E^{(sc)}$. Equations (3.2.10) and (3.2.11) completely specify the neutrino radiation field.

3.3 Rosseland Mean Opacities

Here we are concerned with the total neutrino energy flux emitted from a local surface region of the neutron star.The magnetic field strength in this local region is assumed to be constant. Since the scale heights for physical quantities such as the matter density and temperature are much smaller than the local radii, we adopt the plane-parallel geometry. Integrating equation (3.2.11) over the neutrino energy, we find that the total neutrino energy flux (of a specific species) $F = \int F_E dE = F\hat{r}$ is given by

$$F = -\frac{c}{3\rho\kappa_R}\frac{dU}{dr} \tag{3.3.1}$$

where $U = \int U_E dE$ is the total neutrino energy density, and κ_R is the " Rosseland mean opacity " defined as

$$\frac{1}{\kappa_R} = \frac{\int dE(\frac{1}{\kappa_E^{(t)}})(\frac{dU_E}{dr})}{\int dE(\frac{dU_E}{dr})} \tag{3.3.2}$$

Since neutrino emission and absorption rates are extremely fast even in the regions near the proto-neutron star surface,

a radiative equilibrium approximately holds, i.e.,

$$\int \rho\kappa_E^{(abs)}(U_E^{(FD)} - U_E)dE \simeq 0. \tag{3.3.3}$$

From equation (3.2.10), we have dF/dr $\simeq$ 0, or F is approximately constant.

If we introduce the Rosseland mean optical depth measured from the stellar surface via $d\tau_R = \rho\kappa_R dr$, with F constant, equation (3.3.1) can be integrated to yield

$$cU = 3F(\tau_R + \frac{2}{3}), \tag{3.3.4}$$

where we have used the boundary condition F = cU/2 at the surface ($\tau_R = 0$). Equation (3.3.4) resembles the standard Eddington profile. Note that outside the decoupling region the neutrino energy density U may not be equal to $U^{(FD)} = (7\pi^4/240)T^4$ specified by the matter temperature T . Similarly, U_E may differ substantially from $U_E^{(FD)}(T)$ (see § 3.5). However, we can still approximate U_E

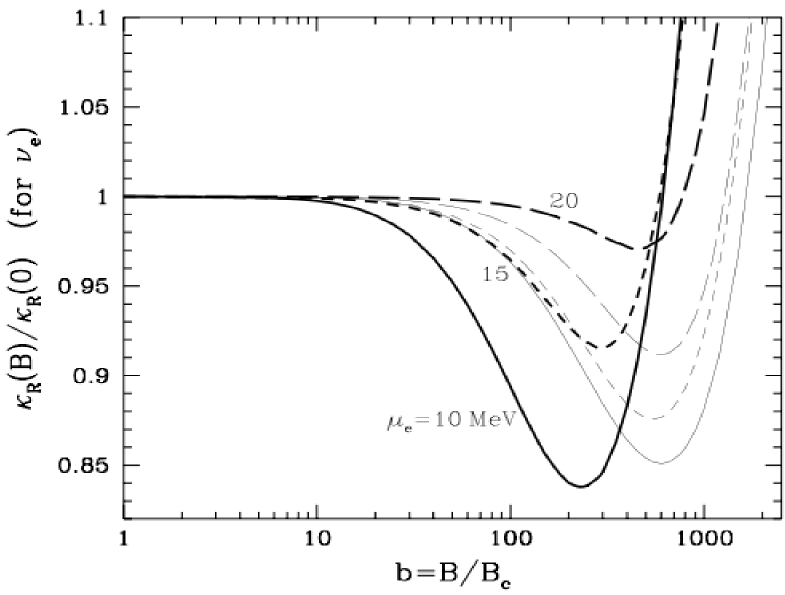

Figure 3.4: Ratio of the Rosseland mean opacity $\kappa_R^{(B)}$ of ν_e to its zero- field value $\kappa_R^{(0)}$ as a function of the magnetic field strength $b = B/B_c$ (with $B_c = 4.414 \times 10^{13}$ G). All results assume $Y_e = 0.1$. The heavier curves correspond to T $=T_\nu = 3$ MeV, and the lighter cures correspond to T $= T_\nu = 5$ MeV. Thel solid, short-dashed, and long-dashed lines are for μ_e = 10, 15, and 20 MeV, respectively.

by the Fermi-Dirac function at the neutrino temperature T_ν, which is equal to the matter temperature at the decoupling layer. Equation (3.3.2) can then be rewritten as

$$\frac{1}{\kappa_R} = \frac{30}{7\pi^4 T_\nu^5} \int dE \frac{1}{\kappa_R^{(t)}} \frac{E^4 exp(E/T_\nu)}{[exp(E/T_\nu) + 1]^2}. \tag{3.3.5}$$

With the cross sections given in § 3.1, we can calculate the Rosseland mean opacity $\kappa_R^{(B)}$ in magnetic fields using equation (3.3.5). Note that in equation (3.3.5) $\kappa_E^{(t)}$ depends on the local matter temperature T . Only in the regions not far from the decoupling layer, do we have T_ν = T .

Figure 3.4 shows the ratio of the Rosseland mean opacity $\kappa_R^{(B)}$ of ν_e to the zero-field value $\kappa_R^{(0)}$ as a function of the magnetic field strength for typical conditions near the proto-neutron star surface. We choose these conditions to be T = T_ν = 3, 5 MeV, and μ_e = 10, 15, 20 MeV, all with $Y_e = 0.1$. Figure 3.5 shows similar results for $\bar{\nu}_e$ with similar physical parameters (T = T_ν = 3, 5, 7 MeV ; Note that the results are insensitive to μ_e). We see that deviation of $\kappa_R^{(B)}$ from the zero-field value by more than 5% generally requires field strength b = $B/B_c \gtrsim 100$.

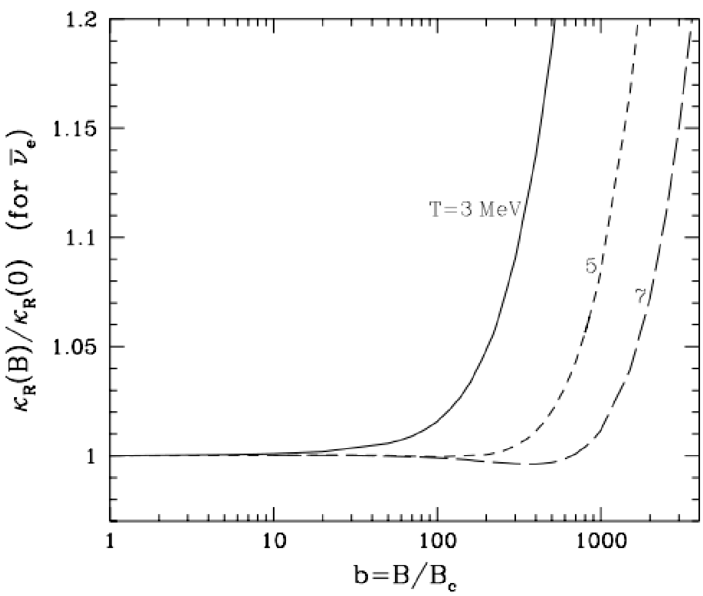

Figure 3.5: Ratio of the Rosseland mean opacity $\kappa_R^{(B)}$ of ν_e to its zero- field value $\kappa_R^{(0)}$ as a function of the magnetic field strength $b = B/B_c$ (with $B_c = 4.414 \times 10^{13}$ G). All results assume $Y_e = 0.1$ and μ_e=20 MeV (but the results are rather insensitive to the value of μ_e). The solid, short-dashed, and long-dashed lines are for T=T_ν = 3, 5, and 7 MeV, respectively.

Note that the results mainly depend on T_ν and are rather insensitive to T.

The behavior of the ratio $\kappa_R^{(B)}/\kappa_R^{(0)}$ as a function of b is certainly not obvious a priori. Since the Rosseland mean integral is dominated by neutrinos with the smallest opacities, and since $\kappa_R^{(abs)}$ scales linearly with B in the regime where only the ground Landau level is filled (see eq. [3.1.17]), we expect that for sufficiently large B, the Rosseland mean opacity increases linearly with increasing B. This is indeed what is indicated in Figures 3.4 and 3.5. For " intermediate " field strength, the $\kappa^{(abs)}$ curve for ν_e (see Fig. 3.1) has a significant portion that is below the zero-field value at low neutrino energies. For such intermediate fields, we would expect $\kappa_R^{(B)}$ to be less than the zero-field value. This explains the nonmonotonic behavior of $\kappa_R^{(B)}/\kappa_R^{(0)}$ as a function of B shown in Figure 3.4. For $\bar{\nu}_e$, the nonmonotonic behavior is much less pronounced (see the curve for T = 7 MeV in Fig. 3.5) since the energy range in which $\kappa_R^{(abs)} < \kappa_R^{(abs)}$=0 is smaller.

3.4 Differential Neutron Fluxes And neutron Star Kick From Asymmetric Magnetic Field Topology

Imagine a proto-neutron star with an asymmetric magnetic field topology, e.g., the north pole and the south pole have different magnitudes of magnetic field (say, by a factor of a few). What is the difference between the neutrino fluxes from these two regions resulting from the different absorption opacities of ν_e and $\bar{\nu}_e$, and what is the resulting kick velocity of the neutron star ? We recall that the fractional asymmetry α in the total neutrino emission (of all species) required to generate a kick velocity V_{kick} is $\alpha= 0.028[V_{kick}/(10^3 kms^{-1})][E_{tot}/(3\times 10^{53} ergs)]$, where E_{tot} is the total neutrino energy radiated from the neutron star (the neutron star mass has been set to $1.4M\odot$). In reality, rotation (if it is misaligned with the magnetic axis) tends to reduce the kick velocity. We also note that the asymmetric ν_e and $\bar{\nu}_e$ emission from the proto-neutron star would give rise to asymmetric neutrino heating behind the stalled shock in the delayed supernova mechanism. This asymmetric heating could lead to asymmetric supernova explosions.

To quantitatively understand how the magnetically modified opacities change the local neutrino flux, we will have to evaluate these opacities at different depths (corresponding to different physical conditions) below the neutron star surface, and to perform complete cooling calculations that take into account these opacities. However, Figures 3.4 and 3.5 clearly indicate that, even near the stellar surface, where one expects the modification to the opacities to be most prominent, and even with the most favorable conditions for the magnetic field to be effective in changing the opacities (i.e., low density and low temperature), a 5% change in the Rosseland mean opacity (for ν_e or $\bar{\nu}_e$) requires a magnetic field with $b \gtrsim 100$, or $B \gtrsim 4\times 10^{15}$ G.

In the following, we shall content ourselves with merely estimating the change in the local neutrino flux from the modified opacities.

We first consider the case in which the matter temperature throughout the neutron star is unaffected by the magnetic field. One might imagine this as a possibility if convection dominates energy transfer between different parts of the star. Under the neutrino-matter decoupling layer the specific neutrino energy density U_E is the same as the Fermi-Dirac function $U_E^{(FD)}(T)$ specified by the matter temperature. The emergent neutrino flux is then inversely proportional to the Rosseland mean optical depth τ_R from the decoupling layer to the stellar surface (see eq. [3.3.4]). Since τ_R for ν_e or $\bar{\nu}_e$ at the decoupling layer is of order a few, the flux F is inversely proportional to κ_R evaluated near the decoupling region. If we use the curve for T = 3 MeV and $\mu_e = 10$ MeV in Figure 3.4 (which has the most pronounced magnetic correction), we find that the fractional change in the ν_e flux is $\delta F_{\nu_e}/F_{\nu_e} \sim 0.1$ at b = 100 (If we had used the curve for $\mu_e = 15$ or l20 MeV, which more closely represents the physical condition at the decoupling region,the modification $\delta F_{\nu_e}/F_{\nu_e}$ would have been smaller by a factor of a few or more). Similarly, using the curve for T = 3 MeV in Figure 3.5 to maximize the magnetic correction, we find $\delta F_{\nu_e}/F_{\nu_e} \sim 0.02$ at b = 100. Since the fluxes of other types neutrinos are unchanged, and since different neutrino species more or less carry away the same amount of energy, the change in the total neutrino flux is only $\delta F_{\nu_e}/F_{\nu_e} \sim 0.01$ at b = 100. If we now imagine that the north pole of the neutron star has $b \sim 100$, while the south pole has a field strength a factor of a few smaller, then, taking into account the geometric reduction ($\sim \frac{1}{3}$), the flux asymmetry is about $\alpha \sim 0.003$, just enough to give a kick velocity of $\sim 100kms^{-1}$ to the neutron star. With κ_R evaluated at more realistic conditions, we expect the resulting α to be even smaller.

The assumption that the matter temperature is unaffected by the magnetic field (and therefore spherically symmetric) is unlikely to be valid. In reality, when a region of the star (say the north pole) emits more flux, it also cools faster. With reduced temperature, this region will tend to emit less flux. In the extreme case, one would find $F \sim cU_o/\tau_R$, with U_o the neutrino energy density in the stellar core, and τ_R the Rosseland mean optical depth from the core to the surface. Since in the bulk interior of the star, modification to κ_R because of the magnetic field is negligible, we would conclude that the change in the neutrino flux is much smaller than what is estimated in the last paragraph. To summarize, the modifications to the absorption opacities of ν_e and $\bar{\nu}_e$ due to quantized Landau levels give rise to rather small change in neutrino fluxes from the neutron star. To generate appreciable kick velocities ($\sim 300kms^{-1}$) from this effect requires the difference of field strengths at the two opposite poles to be at least 10^{16} G (and possibly much larger).

3.4.1 Asymmetric Emission of Neutrinos from a Proto-Neutron star

The inverse beta decay cross-section is direction sensitive through its dependence on the angle θ is known,the angle between the neutrino 3-momentum and the magnetic field direction (see below). This anisotropic effect in the cross-section can have interesting astrophysical applications in explaining the high velocities of pulsars, of the order of 450 $\pm$ 90 km s^{-1}. Typical pulsars have masses between $1.0M_\odot$ and $1.5M_\odot$,i.e., about $2\times\ 10^{33}$g. The momentum associated with the proper motion of a pulsar would therefore be of order 10^{41} g cm/s. On the other hand the energy carried off by neutrinos in a supernova explosion is about $3\times\ 10^{53}$ erg, which corresponds to a sum of magnitudes of neutrino momenta of 10^{43} g cm/s. Thus an asymmetry of order of 1% in the distribution of the out going neutrinos would explain the kick of the pulsars [This is our goal]. It has been suggested [28,29,30] that an asymmetry of this order in the distribution of outgoing neutrinos can be generated by the anisotropic cross-sections of the various neutrino related processes in presence of a constant magnetic field. A simple calculation given below makes this point clear.

The typical size of a neutron star is about R $\approx$ 10 km . Thus, when a neutrino, generated at the core reaches a density where its mean free path is about R, it escapes from the star. Therefore the condition for the neutrino to escape can be written as

$$n_n \sigma = 1/R, \tag{3.4.1}$$

where n_n is the neutron number density. We already observed that σ is direction dependent. Therefore, the value of n_n on the " neutrino sphere " depends on the direction as well, and the surface is no longer a sphere. Different values of n_n will correspond to different tempertures. Thus, neutrinos will be emitted with different momenta in different directions. This can result in a kick to the star.

It is known that [31,32] the scattering cross-section for the inverse beta decay processes is given by

$$\sigma = \sum_{n'=0}^{n'_{max}} \sigma_{n'} = \frac{eBG_B^2}{2\pi} \sum_{n'=0}^{n'_{max}} \Big[g_{n'} \{ (G_V^2 + 3G_A^2) + 2G_A \delta (G_V + G_A) cos\theta \} + \delta_{n'}, 0$$

$$+ \delta_{n'}, 0 \{ (G_V^2 - G_A^2) cos\theta + 2G_A \delta (G_V - G_A) \} \Big] \times \frac{k + E_\nu}{\sqrt{(k + E_\nu)^2 - m^2 - 2n'eB}}, \tag{3.4.2}$$

$(k + E_\nu)^2 - m^2 - 2n' eB = 0$, positive

$$n'_{max} = \frac{(k + E_\nu)^2 - m^2}{2eB} \tag{3.4.3}$$

where, k=$\sqrt{\frac{E_n + m}{E_n}}$ and E_ν = neutrino energy.

Rearrange equation (3.4.2),

when $g_{n'}$=1 and n'=0,

$$\sigma = \frac{eBG_B^2}{2\pi} [(G_V^2 + 3G_A^2) + (G_V^2 - G_A^2) cos\theta] \tag{3.4.4}$$

and,

$$a = \frac{G_V^2 + 3G_A^2}{2\pi}, \quad and \quad b = \frac{G_V^2 - G_A^2}{2\pi}, \tag{3.4.5}$$

which can be put in the form of

$$\sigma = eBG_B^2 (a + bcos\theta). \tag{3.4.6}$$

This can be to estimate the magnitude of the kick, we abbreviate the electron-neutrino cross-section. If we now cosider the directions $\theta = 0$ and $\theta = \pi$, combined with equation (3.4.1 and 3.4.5) the difference in neutron density on the corresponding points on the neutrino surface is given by

$$\Delta n_n = 1/eBG_B^2R[1/(a-b) - 1/(a+b)] = 2b/(eBG_B^2a^2R), \tag{3.4.7}$$

neglecting corrections of order b/a.

The neutron gas in a typical proto-neutron star can be considered to be non-relativistic and degenerate. The number density of neutrons is thus given by

$$n_n = p_F^3/3\pi^2[1 + (\pi^2 m_n^2 T^2/p_F^4) + ...], \tag{3.4.8}$$

where p_F is the Fermi momentum, and we have neglected higher order terms in the temperature. In equation (3.4.4) differetiate by tempreture, this gives

$$dn_n/dT = m_n^2/3(T^2/p_F) \tag{3.4.9}$$

Substitute equation (3.4.6) into equation (3.4.8), So the temperature difference between the points on the neutrino surface in the $\theta = 0$ and $\theta = \pi$ directions is

$$\Delta T = 3/m_n^2(p_F/T^2)(2b/eBG_B^2a^2R). \tag{3.4.10}$$

The momentum asummetry can now be written as

$$\Delta|q|/q = 1/6(4\Delta T), \tag{3.4.11}$$

where we have assumed a black body radiation luminosity ($\propto T_4$) for the effective neutrino surface. The factor 1/6 comes in because the asymmetry pertains only to ν_e, where as 6 types of neutrinos contribute to the energy emitted equation (3.4.9) and equation (3.4.10) are combined. This gives

$$\Delta|q|/q = 4/m_n^2(p_F/T^2)(b/eBG_B^2a^2R). \tag{3.4.12}$$

To find p_F, we use the leading term in the expansion for n_n given above and estimate n_n from the equation

$$n_n = \rho(1 - Y_e)/m_p, \tag{3.4.13}$$

where Y_e is the electron fraction and ρ is the mass density. Taking $Y_e = 1/10$, we obtain

$$p_F = 24\rho_{11}^{1/3} MeV. \tag{3.4.14}$$

where ρ_{11} is the mass density in units of 10^{11} gcm^{-3}. Putting this back in the ratio $\Delta|q|/q$ just given above we obtain

$$|\Delta|q|/q| = 27\rho_{11}^{1/3} B_{14}^{-1} T^{-2} MeV(|b|/a^2), \tag{3.4.15}$$

where, $B_{14} = B/(10^{14} Gauss)$ and T_{MeV} = T/(1MeV). For $\Omega \gg m_e$ which is the relevant case and S = 0 as a typical values of neutron polarization, we can find out the values of the constants a and b. The values of both of them will in general depend upon n'_{max} (the maximum allowed Landau number), but if we take only the contribution from the $n' = 0$ level then

a = $(G_V^2 + 3G_A^2)/2\pi$ = 9.2 × 10^{-1},

and

b = $(G_V^2 - G_A^2)/2\pi$ = -9.3 × 10^{-2}

using $G_V = 1$ and $G_A = 1.26$

This gives

$$|\Delta|q|/q| = 3\rho_{11}^{1/3} B_{14}^{-1} T^{-2} MeV. \tag{3.4.16}$$

Obviously, with reasonable choices of ρ,B and T, it is possible to obtain a fractional momentum imbalance of the order of 1% which is necessary for explaining the pulsar kicks.

The momentum associated with the proper motion of a pulsar would there be of order 10^{41} $gcms^{-1}$ and the sum of magnitudes of neutrino momenta of 10^{43} $gcms^{-1}$.

The ratio of $|\Delta|q|/q|$ = 10^{41} $gcms^{-1}$/ 10^{43} $gcms^{-1}$=1%

when, ρ_{11} = 7.2 × 10^{11} gcm^{-3}

T = 3 MeV = 3 × 10^6 eV

B_{14} = B/10^{14}G

So, this values substitute in equation (3.4.15), we get

$B = \frac{3(7.2\times10^{11})(10^{14})(10^2)}{9\times10^{12}}$ G

$\therefore$ B = 2.4 $\times$ 10^{15}G.

This is our estimated magnetic field.

3.5 Magnetic Field Effect On ν_e And $\bar{\nu}_e$ Energy Spectra

We now consider how the oscillatory behaviors (see Figs. 3.1-3.3) of the absorption opacities of ν_e and $\bar{\nu}_e$ may manifest themselves in the radiated neutrino energy spectra. For an absorption dominated medium, neutrinos with energy E decouple from the matter and start free-streaming at a column depth (in g cm^{-2}) y = $\int \rho dr \sim 1/\kappa_R^{(abs)}$. Thus, the neutrino energy spectrum is given by $F_E \sim cU_E^{(FD)}$ with $U_E^{(FD)}$ evaluated at the depth $y \sim 1/\kappa_E^{(abs)}$. In the presence of significant scattering, decoupling occurs at depth $y \sim 1/\kappa_E^{eff}$ with the effective opacity $\kappa^{eff} \sim (\kappa_E^{(abs)}\kappa_E^{(t)})^{1/2}$, where as the neutrinosphere from which neutrinos start free-streaming is located at $y \sim 1/\kappa_E^{(t)}$. Near the decoupling region we have $dU_E/dr \sim \rho\kappa_E^{eff}U^{(FD)}$, and thus from equation (3.2.11) the neutrino spectral energy flux is given by

$$F_E \sim \frac{\kappa_E^{eff}}{\kappa_E^{(t)}} cU_E^{(FD)}\left(y \sim \frac{1}{\kappa_E^{eff}}\right). \tag{3.5.1}$$

The above qualitative argument can be made more rigorous by directly solving equations (3.2.10) and (3.2.11). Consider a plane parallel atmosphere and define the (energy dependent) optical depth via $d\tau_E = -\rho\kappa_E^{(t)}dr = \kappa_E^{(t)}dy$. Equations (3.2.10) and (3.2.11) can be combined to give

$$\frac{d^2}{d\tau_E^2}U_E = \beta_E^2[U_E - U_E^{(FD)}], \quad with \;\; \beta_E^2 = 3\frac{\kappa_E^{(abs)}}{\kappa_E^{(t)}}. \tag{3.5.2}$$

with a constant β_E, the above equation can be solved exactly. For the boundary condition $F_E = (c/3)(dU_E/d\tau_E) = cU_E/2 \;\; at \;\; \tau_E = 0$, the neutrino energy flux at the surface is given by

$$F_E = \frac{\beta_E/3}{1+2\beta_E/3}\int_0^\infty d\tau_E \beta_E c U_E^{(FD)}(\tau_E) exp(-\beta_E \tau_E)$$
$$\simeq \frac{\beta_E/3}{1+2\beta_E/3} cU^{(FD)}(\tau_E \simeq \beta_E^{-1}). \quad (3.5.3)$$

Figure 3.6 shows the spectral energy fluxes of ν_e calculated using equation (3.5.3) for different field strengths (b = 100 and 300). The matter temperature profile is obtained from equation (3.3.3) assuming $U \propto T^4$. For a total energy flux of $F = (c/4)U(T_{eff})$ (where T_{eff} is the effective temperature), we have T $= T_{eff}[(\frac{3}{4})\tau_R + \frac{1}{2}]^{1/4}$. We choose T_{eff} = 3 MeV in these examples. For simplicity, we have neglected the variations of the opacities as a function of τ_E . Thus, the temperature at decoupling ($\tau_E \simeq \beta_E^{-1}$; see eq.[3.5.3]) is given by T$\simeq$ $T_{eff}[(\frac{3}{4})\kappa_R/\kappa_E^{(eff)} + \frac{1}{2}]^{1/4}$, where $\kappa_E^{(eff)} = \beta_E \kappa_E^{(t)} = (3\kappa_E^{(abs)}\kappa_E^{(t)})^{1/2}$, and we take the relevant opacities to have the corresponding values for $Y_e = 0.1$, $\mu_e = 20$MeV.and T=3MeV. This simplification should not introduce qualitative changes in the spec-

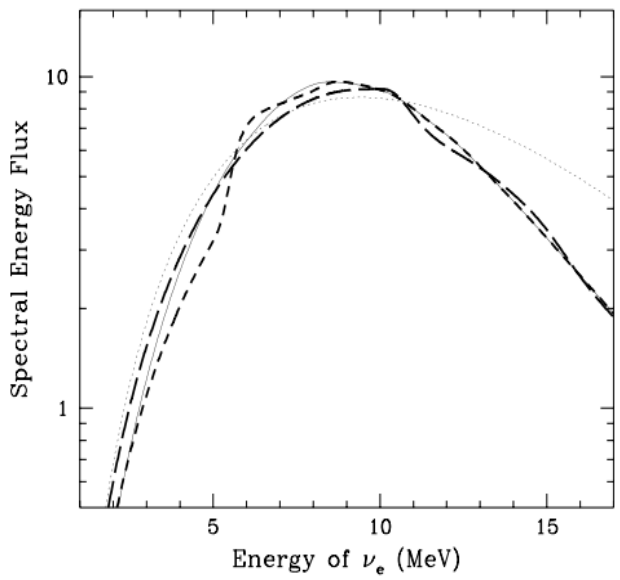

Figure 3.6: Illustrative examples of the ν_e spectral energy fluxes (in arbitrary units) modified by the magnetic fields. The light solid, short-dashed,and long-dashed lines are for b = 0, 100, and 300, respectively. The light dotted line is the Fermi-Dirac spectrum with T = T_{eff} = 3 MeV.

trum. As seen from Figure 3.6, the spectrum is pinched at the high energies because of the E^2- dependence of the opacities. The magnetic field introduces modulations in the spectrum. For lower magnetic field strengths, the modulations occur at the lower energy band. As the magnetic field gets stronger, the modulations shift to the higher energy part of the spectrum.

The distortions and modulations of the ν_e and $\bar{\nu}_e$ energy spectra by strong magnetic fields may offer an interesting possibility to limit the magnetic field strength in proto- neutron stars through the detection of neutrinos from a Galactic supernova. We note, however, that the ν_e spectra shown in Figure 3.6 are based on very approximate calculations. They serve only as illustrative examples of the magnetic field effect on the neutrino spectra. More detailed calculations are needed to obtain realistic spectra that include the magnetic field effect.

Chapter 4

Conclusion

In this thesis, We have discussed first detection of γ-ray pulsations from an individual globular cluster MSP (PSR J1823-3021A). Whose γ-ray luminosity is among the highest observed for any MSP. The pulsar dominates the total emission of the cluster. The issue of whether asymmetric magnetic field topology in a proto-neutron star can induce asymmetric neutrino emission from the star through the modifications of the neutrino absorption opacities by the magnetic field. Another related (but distinct) kick mechanism relies on the fact that ν_e and $\bar{\nu}_e$ absorption opacities near the neutrinosphere depend on the local magnetic field strength (because of the quantization of e^- and e^+ energy levels). If the magnitude of the magnetic field in the north pole is different from that in the south pole, then asymmetric neutrino flux can be generated. We show in Lai and Qian (1998b) that this kick mechanism requires a much larger field strength. These modifications arise from the quantized Landau levels of electrons and positrons produced in strong magnetic fields. By calculating the appropriate mean neutrino opacities in the magnetic field, we demonstrate that this mechanism is rather inefficient in generating a kick to the neutron star : To obtain appreciable kick velocities ($\sim 300kms^{-1}$), the difference between the field strengths at the two opposite poles of the star must be at least 10^{16} G. The inverse beta-decay process, even for unpolarizied Neutrons (S=0), the cross-section depends on the direction of the neutrino momemtum (anisotropy in the cross-section). The anisotropy in the cross-section comes only from the zeroth Landau level contribution of the electron. However, for the higher levels, there is a cancellation beteewn the two possible states in a Landau level which washes out all angular dependence in these levels, provided the neutrons are unpolarized. The asymmetry in cross-section will therefore come only from the zeroth Landau level state of the electrons and its amount will depend on the relative contribution of this state to the total cross-section. If the magnetic field is so high that only the zeroth Landau level state can be obtained for the electron, the asymmetry will be large, about 18%. For smaller and smaller magnetic fields, the asymmetry decreases with new Landau levels contributing. For polarized neutrons, however,there is an asymmetry even in the field-free case.

References

[1] Biggs,J.D., Lyne,A.G.,Manchester,R.N.,and Ashworth,M.1990,IAU Circ.,4988,2

[2] Akhmedov, E. K., Lanza, A., and Sciama, D. W. 1997, Phys. Rev. D, 56, 6117.

[3] Arras, P., and Lai, D. 1998, Phys. Rev. Lett., submitted (astro-ph/9806285).

[4] Aschenbach, B., Egger, R., and Trumper, J. 1995, Nature, 373, 587.

[5] Bazan, G., and Arnett, D. 1994, ApJ, 433, L41.

[6] Bezchastnov, V. G., and Haensel, P. 1996, Phys. Rev. D, 54, 3706.

[7] Bisnovatyi-Kogan, G. S. 1993, Astron. Astrophys. Trans., 3, 287.

[8] Brandt, N., and Podsiadlowski, P. 1995, MNRAS, 274, 461.

[9] Burrows, A., and Fryxell, B. A. 1992, Science, 258, 430.

[10] Chugai, N. N. 1984, Soviet Astron. Lett., 10, 87.

[11] Cordes, J. M., Wasserman, I., and Blaskiewicz, M. 1990, ApJ, 349, 546.

[12] Cropper, M., et al. 1988, MNRAS, 231, 695.

[13] Deway, R. J., and Cordes, J. M. 1987, ApJ, 321, 780.

[14] Dorofeev, O. F., et al. 1985, Sov. Astron. Lett., 11, 123.

[15] Frail, D. A., Goss, W. M., and Whiteoak, J. B. Z. 1994, ApJ, 437, 781.

[16] Gott, J. R., Gunn, J. E., and Ostriker, J. P. 1970, ApJ, 160, L91.

[17] Hansen, B. M. S., and Phinney, E. S. 1997, MNRAS, 291, 569.

[18] Horowitz, C. J., and Li, G. 1997, preprint (astro-ph/9705126).

[19] Iben, I., and Tutukov, A. V. 1996, ApJ, 456, 738.

[20] Kaspi, V. M., et al. 1996, Nature, 381, 584.

[21] Lai, D., and Qian, Y.-Z. 1998, ApJ, 495, L103.

[22] Lorimer, D. R., Bailes, M., and Harrison, P. A. 1997, MNRAS, 289, 592.

[23] Lyne, A. G., and Lorimer, D. R. 1994, Nature, 369, 127.

[24] Morse, J. A., Winkler, P. F., and Kirshner, R. P. 1995, AJ, 109, 2104.

[25] Taylor, J. H., and Cordes, J. M. 1993, ApJ, 411, 674.

[26] Vilenkin, A. 1995, ApJ, 451, 700.

[27] Ziman, J. M. 1979, Principles of the Theory of Solids (Cambridge Univ.Press : Cambridge), 319.

[28] O.F.Dorofeev,V.N.Rodionov and I.M.Ternov,JETP Lett.40,917(1984)[Pisma Zh.Eksp.Tero.Fiz.40,159(1984)].

[29] G.S.Bisnovatyi-Kogan,Astron.Astrophys.Trans.3,287(1993)[arXiv:astroph/9707120].

[30] A.Goyal,Phys.Rev.D 59,101301(1999)[arXiv:hep-ph/9812473].

[31] Dong Lai, Y. -Z. Qian astro-ph/9802345 (February 1998).

[32] Kaushik Bhattacharya, Palash B. Pal hep-ph/0209053 (2002).

Declaration

I here by declare that this thesis is my original work and has not been presented for a degree in any other university. All sources of material used for the thesis have been duly acknowledged.

Name: Tesfaye Teklehaimanot

Signature: ....

This thesis has been submitted for the examination with my approval as university advisor.

Name: Dr.Legesse Wotro K.

Signature: ....

Addis Ababa University

Department of Physics

June, 2013